



HAL
open science

Evaluation of Magnetic Behavior of a Single Pole Pair Fe-Cr-Co-based Memory Motor Considering a Standstill Magnetization

Flavia Domingues de Sousa, Alexandre Battiston, Farid Meibody-Tabar,
Serge Pierfederici

► To cite this version:

Flavia Domingues de Sousa, Alexandre Battiston, Farid Meibody-Tabar, Serge Pierfederici. Evaluation of Magnetic Behavior of a Single Pole Pair Fe-Cr-Co-based Memory Motor Considering a Standstill Magnetization. IEEE Transactions on Magnetics, 2022, 58 (8), pp.1-7. 10.1109/TMAG.2022.3141895 . hal-03777715

HAL Id: hal-03777715

<https://ifp.hal.science/hal-03777715>

Submitted on 15 Sep 2022

HAL is a multi-disciplinary open access archive for the deposit and dissemination of scientific research documents, whether they are published or not. The documents may come from teaching and research institutions in France or abroad, or from public or private research centers.

L'archive ouverte pluridisciplinaire **HAL**, est destinée au dépôt et à la diffusion de documents scientifiques de niveau recherche, publiés ou non, émanant des établissements d'enseignement et de recherche français ou étrangers, des laboratoires publics ou privés.

Evaluation of the Magnetic Behavior of a Single Pole Pair Fe-Cr-Co-based Memory Motor Considering a Standstill Magnetization

Flávia Domingues de Sousa¹, Alexandre Battiston¹, *Member, IEEE*, Farid Meibody-Tabar², and Serge Pierfederici²

¹IFP Energies nouvelles - Institut Carnot IFPEN Transports Energie, Rueil-Malmaison 92852, France

²Laboratoire LEMTA, Université de Lorraine, Vandœuvre-Lès-Nancy 54500, France

Variable Flux Memory Machines (VFMM) can have their level of magnet flux density modified by the injection of d-axis current pulses in the armature windings. The use of Fe-Cr-Co magnets as source of the magnetic field in these machines is still little explored, even if these magnets present interesting thermal and mechanical proprieties. In this context, this paper explores the validation of a standstill magnetization strategy applied in a non-salient single pole pair Fe-Cr-Co-based VFMM designed for high-speed applications in the transportation electrification field. Due to the absence of a well-defined knee on the second quadrant of the hysteresis loop of the magnet used, the methodology commonly seen in the literature for describing the behavior of the recoil lines defining the working points cannot be directly used. Therefore, by the experimental results obtained from the standstill magnetization of the VFMM studied, a new methodology is developed based on the estimation of the remanence in terms of the excitation field characterizing the internal hysteresis loops of the Fe-Cr-Co. The achieved results are compared with the reference obtained from a HysteresisGraph, which represents a closed and ideal magnetic circuit of measurement. The effects of a stator geometry designed with closed slot wedges in the VFMM and the anisotropy shape are explored for justifying the differences observed.

Index Terms—Fe-Cr-Co Magnets, Memory Machines, Standstill Magnetization, Variable Flux Memory Machines.

I. INTRODUCTION

VARIABLE Flux Memory Machines (VFMM) [1] present as major feature an adjustable air gap flux density. Current pulses are injected in the armature windings along the magnetization axis allowing these machines to operate under dynamically changing load conditions [2], in a wider torque-speed range envelope. Particularly for operations above the base speed, the possibility of using short-time magnetization currents for demagnetizing the low coercive force (LCF) magnet is an advantage. It reduces the copper losses generated by flux-weakening strategies required when permanent magnet synchronous machines (PMSMs) are used under the same operating conditions [3], [4].

The risks of supply, price variability [5] and the challenges related to their extraction, refinement, and recycling [6], [7] are the main concerns related to the use of rare-earth magnets (REMs). VFMMs emerged as an option to reduce the use of these materials. The use of Al-Ni-Co as LCF magnets in these machines has been explored by many authors due to their high remanent flux density and good thermal proprieties [1], [8]. However, similar materials as Fe-Cr-Co are still little explored. Even so, characteristics as higher Currie temperatures, their mechanical resistance and lower Cobalt content can be interesting for electrical machines in terms of cost and performance [9].

This paper is focused on single-type AC-magnetized single pole design composed of a solid cylindrical Fe-Cr-Co-based rotor. A review in VFMM topologies is presented in [2], [10]. The variation of the magnetization level of the magnet is proposed by injecting current pulses in the stator windings at standstill. Results obtained from the back-EMF measured after each magnetization process are used for understanding the behavior of the recoil lines characterizing the magnet used in the machine. A similar approach is presented in [11] for

studying the effects of using different d-axis pulses widths and amplitudes in the magnetization process of an Al-Ni-Co-based VFMM. However, the linear model seen in the literature for defining the behavior of the minor hysteresis loops of Al-Ni-Co magnets [12], [13] cannot be directly used for the Fe-Cr-Co magnet studied in this paper, due to the absence of a well-defined knee in the major hysteresis loop (or B-H-loop). Therefore, a new methodology is proposed for estimating the minor loops and consequently the recoil lines defining the working point achieved after each standstill magnetization.

II. THE VARIATION OF THE MAGNETIZATION STATE IN VARIABLE FLUX MEMORY MACHINES

A. Presentation of the machine geometry

The machine stator used in this study was initially designed for a permanent magnet synchronous machine (PMSM). This PMSM is transformed into a VFMM only by replacing a Nd-Fe-B-based rotor by a Fe-Cr-Co-based rotor, with no modifications on the stator geometry. A cylindrical shape for

TABLE I
DESIGN SPECIFICATIONS OF THE VARIABLE FLUX MEMORY MACHINE

Air gap thickness (mm)	0.5
Fe-Cr-Co magnet length (mm)	18.1
Fe-Cr-Co magnet diameter (mm)	17
Number of slots	12
Number of spires	1 per pole and per phase

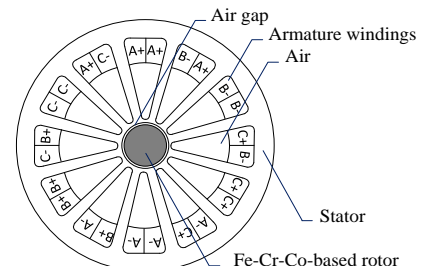


Fig. 1. Design of the proposed Fe-Cr-Co-based Variable Flux Memory Machine

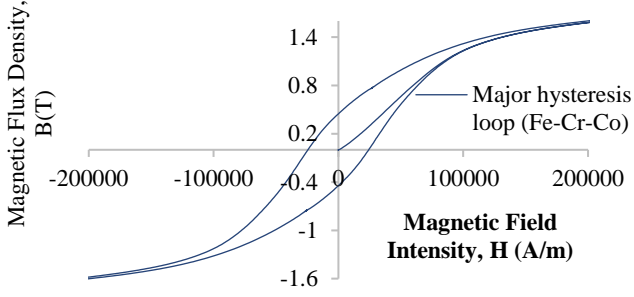


Fig. 2. Hysteresis loop of the Fe-Cr-Co obtained by experimental tests using the HysteresisGraph

the magnet is used to reduce the fragility in high-speed operations and to make easy the adaptability to other stator geometries.

The stator is composed by standard NO20 electrical steel forming 12 teeth. The Fig. 1 presents the design described and the Table I the design specifications. A sample of Fe-Cr-Co magnet is characterized using a HysteresisGraph, a closed and ideal magnetic circuit of measurement [14], [15]. In the Fig. 2, the major hysteresis loop obtained from the magnet characterization is exhibited. A coercivity (H_c) of -24.4kA/m and a remanence (B_r) of 0.45T can be identified.

B. Description of the operating principle of the machine

The working point of variable flux memory machines, in the B_m - H_m plan, is located at the intersection of the hysteresis loop of the magnet and the load line defined when this same magnet is inserted in a magnetic circuit. The slope of this load line, estimated by the expression $B_m=f(H_m)$ given by (1), depends on the machine geometry, but its placement varies according to the amplitude of magnetization (d-axis) current ($I=I_{\text{mag}}$) supplying the armature windings.

$$B_m = -\mu_0 \left(\frac{l_m}{l_g} \right) \left(\frac{A_g}{A_m} \right) H_m + \mu_0 \left(\frac{1}{l_g} \right) \left(\frac{A_g}{A_m} \right) N I_{\text{mag}} \quad (1)$$

$$B_m = k_1 H_m + k_2$$

where B_m (in T) is magnetic flux density, H_m (in A/m) is the magnetic field intensity, A_m (in m^2) is the cross-section area and l_m (in m) is the length of the magnet. The length and the cross-section area of the air gap are respectively given by l_g (in m) and A_g (in m^2). The permeability of vacuum by μ_0 (in H/m) and N is the number of turns of the armature windings in which the magnetization current I_{mag} (in A) is injected.

If the magnetization current is null, equation (1) is reduced to $B_m = k_1 H_m$, a linear equation of negative slope which value

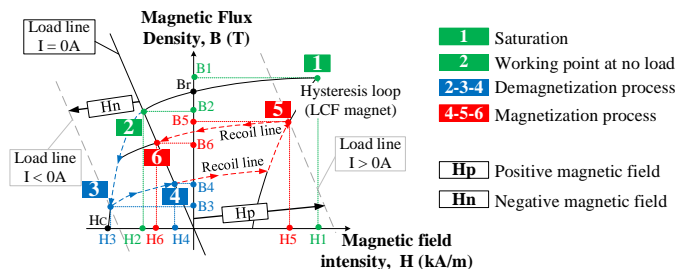


Fig. 3. Theoretical regulation of the working point placement in a VFMM

depends on the machine parameters. If I_{mag} and consequently k_2 are non-zero, the placement of the load line changes. The Fig. 3 presents the theoretical variation of the working point and therefore of the magnetization state (MS) of the magnet, according to the magnetization current amplitude, as also discussed in [2]. From the saturation of the magnet (MS=100%) in the point 1, the working point moves along the external demagnetization curve until point 2 when the magnetization current is suppressed. The working point 2 defines the intersection of the major hysteresis loop and the load line $I_{\text{mag}}=0\text{A}$. From this point, negative current pulses ($I_{\text{mag}}<0$) are injected in the armature windings. The load line is displaced to the left by the also negative external magnetic field created (H_n), reducing the MS of the magnet. This load line intercepts the major B-H-loop in the point 3. When the current is removed, the trajectory of the working point does not retrace the path defined by the points 2-3. Instead of it, it moves along a recoil line until the point 4. A portion of the initial MS of the magnet is conserved even after the demagnetization, which defines the memory of this machine. From the point 4, positive magnetization current pulses ($I_{\text{mag}}>0\text{A}$) creating a positive external field (H_p), displaces the load line $I_{\text{mag}}=0\text{A}$ to the right. The working point traces the path defined by the points 4-5 and then moves to the point 6, when the current is suppressed. Again, the initial MS is partially conserved. It should be observed that the hysteresis loop in the Fig.2 is different to the theoretical one shown in the Fig.3, specially because a well-defined knee is present in the second quadrant of this last mentioned. This difference will be later discussed in this paper.

Based on the simplifying assumption of a linear behavior of the hysteresis loop (Fig.2) in the second quadrant, the level of magnet flux density according to this curve can be defined by:

$$B_m = \mu_0 \mu_r H_m + B_r \quad (2)$$

where μ_r the relative permeability of the LCF magnet and B_r (in T) the remanence. Using (1) and (2), the working point of the magnet can be calculated, which represents the intersection between the major hysteresis curve and the load line $I_{\text{mag}}=0\text{A}$ can be calculated by:

$$B_m = \frac{A_g l_m B_r + \mu_0 \mu_r A_g (N I_{\text{mag}})}{A_g l_m + \mu_r l_g A_m} \quad (3)$$

In [16], the mathematical modelling of the VFMM presented in this paper have been further studied.

C. Description of standstill magnetization procedure

The direction and amplitude of the resultant magnetic field used to modify the MS of the Fe-Cr-Co-based rotor is controlled by the current pulses I_{mag} flowing through the armature windings. A power electronic drive system composed of a two-level voltage source inverter (VSI) is proposed for regulating these currents. A customized software is developed for injecting currents pulses in DC/DC mode without supplementary components and with no neutral access. Fig. 4 shows the basic schema of the drive system. The magnetization current I_{mag} is regulated by controlling one of the inverter's leg

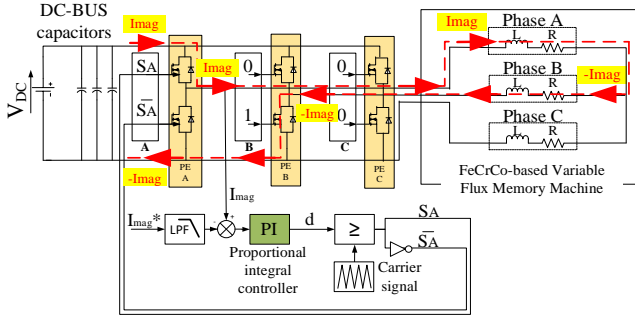


Fig. 4. Drive system for injecting the magnetization current pulses ($I_A=I_{mag}$, $I_B=-I_{mag}$, $I_C=0$) in the armature windings during the experimental tests

while the low-side components of another phase is forced to be turned-on. The third leg of the inverter is not used. The current pattern is defined as $I_A=I_{mag}$, $I_B=-I_{mag}$, $I_C=0$. The PI controller can be regulated using a compensation poles method according to the transfer function of the system defined between I_{mag} and the duty cycle of first inverter's leg switches d . A first order transfer function is obtained for modelling the response of the control system in a closed loop.

Multiple pulses of different amplitudes and time duration of 500ms are used to supply the armature windings at standstill aiming to magnetize the magnet. The machine is then run at 45krpm to evaluate the MS achieved. The flux linkage can be calculated by (4) using the back-EMF measured at the previously described regime.

$$E = N\omega k_m \lambda_m = \omega \lambda_s \quad (4)$$

where E (in V_{pp}) is the measured amplitude of the phase back-EMF supposed being sinusoidal, ω (in rad/s) the electrical speed of the rotor, λ_m (in Wb) the amplitude of the magnet flux, k_m the winding factor, that depends on the machine geometry and the distribution of the windings in the slots, and λ_s (in Wb) the amplitude of the flux linkage through each phase winding. After each magnetization procedure, negative current pulses are used to demagnetize the magnet. The obtained results can be analyzed in the Fig. 5. The Fig. 6 presents the peak-to-peak phase back-EMF measured at $\omega=45$ kpm during the experimental tests after magnetization of the VFMM by $I_{mag}=800$ A. Considering the waveform observed, the back-EMF is assumed as sinusoidal. This premise is going to be later validated by simulations.

D. Validation of standstill magnetization procedure

As previously presented by the Fig. 2, the hysteresis loop characterizing the Fe-Cr-Co used in the VMM studied Fig.3 do not present a well-defined knee in the second quadrant. Therefore, even if this material presents similar proprieties to the ones of Al-Ni-Co magnets as previously discussed, their B-H-loop cannot be compared. An illustrative schema is shown in the Fig. 7 to demonstrate the difference between the magnetic behavior of these two materials. As discussed in [2] and [8], Al-Ni-Co magnets have all their minor hysteresis loops defined with a level of coercivity equals to the one of the major loop. As consequence, the recoil lines are all parallel to the linear portion of the external demagnetization curve, defined in the Fig. 7 by the points 1 and 2. As the hysteresis loop of the Fe-Cr-Co magnet do not present this same linear portion observed

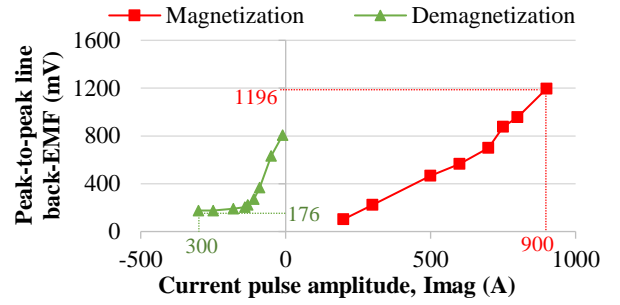


Fig. 5. Measured peak-to-peak line back-EMF for different magnetization/demagnetization current amplitudes by experimental tests

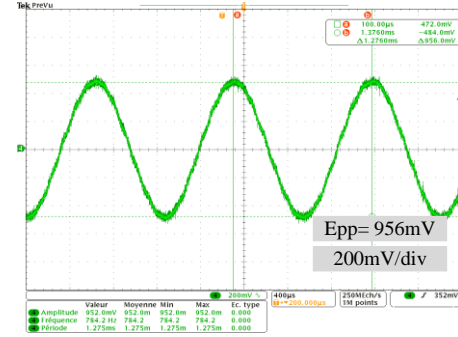


Fig. 6. Back-EMF measured at $\omega=45$ krpm during the experimental tests after magnetization at standstill by $I_{mag}=800$ A

for the Al-Ni-Co, the methodology used validating the results of VFMMs composed of this last mentioned magnet is not applicable for the Fe-Cr-Co-based ones. For this reason, a new methodology is proposed in this paper for defining the behavior of the recoil lines in the hysteresis loop shown in the Fig. 2. The objective is to define the working point placement in this curve when magnetization currents of different amplitudes are used to supply the armature windings of the VFMM described in the Fig. 1.

The parallelism between the recoil lines and the major demagnetization curve in the second quadrant of the hysteresis loop, exhibited between the points 3 and 4 in the Fig. 7, is going to be the basis of this new model. First, from each back-EMF measured during the experimental tests (presented in the Fig. 5), equation (4) is used to calculate the flux linkage λ_s . In a second step, the parameters characterizing the internal recoil lines of the Fe-Cr-Co magnet in the second quadrant of the B-H-loop are going to be estimated by Finite Element Analysis (FEA) simulations. First, the relative permeability of the external demagnetization loop is calculated considering the hypothesis of linearization of the second quadrant of B-H-loop of the Fe-Cr-Co exhibited in the Fig. 2. Using (2), a relative

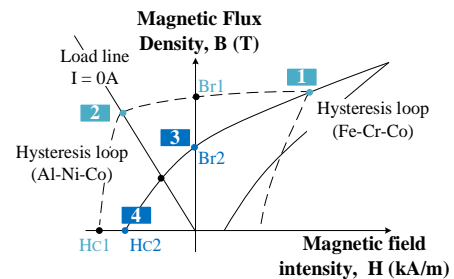


Fig. 7. Illustration for comparison of the hysteresis loop of both Al-Ni-Co and Fe-Cr-Co magnets

TABLE II
CHARACTERIZATION OF THE RECOIL LINES

Experimental Tests		FEA simulations - hypothetical magnets of $\mu_r=14.65$		FEA simulations - initial magnetization curve
d-axis currents [A _{pk}]	Flux linkage [μ Wb]	Coercivity [A/m]	Remanence [T]	Excitation field [A/m]
500	27.95	3900	0.072	84216
600	34.33	4900	0.090	87463
700	42.45	6000	0.110	89182
750	52.32	7300	0.134	90041
800	57.10	8000	0.147	90900
900	71.44	9700	0.179	93622

permeability $\mu_r=14.65$ can be calculated from the values of the remanence of B_r and the coercivity H_c fixed respectively at 0.45T and at -24.4kA/m. For modelling the behavior of each recoil line, considered parallel to the major hysteresis loop, hypothetical materials are characterized by the previously calculated $\mu_r=14.65$ and used in the simulations by FEA to replace the Fe-Cr-Co composing the rotor of the VFMM studied. The coercivities of these hypothetical materials representing the recoil lines are estimated to ensure a flux through the stator windings equals to the ones calculated from the back-EMF measured during the experimental tests by (4). Then, from these values of H_c , the remanences defining each recoil line can be calculated using (2) for $H_m=H_c$ and $B_m=0$. As previously discussed, these results (pairs of H_c , B_r) define the behavior of the recoil lines of the Fe-Cr-Co in the second quadrant of the hysteresis loop and are exhibited in the Table II, for $I_{mag}>400A$. The ratio between the remanences of an internal and the major hysteresis loops can be used to evaluate the magnetization state (MS) of the magnet. Based on the results presented in the Table II, it can be observed that a MS of 39.8% is achieved for $I_{mag}=900A$.

In the third step of the methodology proposed, the behavior of the recoil lines in the first quadrant of the hysteresis loop is defined. For this, data presented in the Fig. 2 for the initial magnetization curve are used for modelling the rotor during

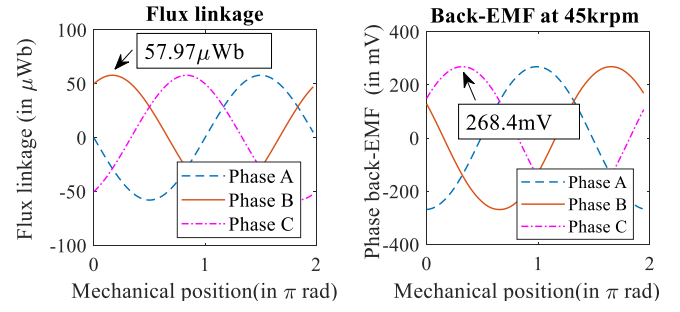


Fig. 9. Flux linkage (left) and back-EMF(right) obtained by characterizing the rotor in FEA simulations considering the recoil line obtained from the methodology proposed for $I_{mag}=800A$.

simulations by FEA. The objective was to estimate, by simulations, the excitation field (H_{exc} , in A/m) in the magnet when the different amplitudes of magnetization current were injected in the armature windings during the experimental tests. A current pattern of $I_A=I_{mag}$, $I_B=-I_{mag}$, $I_C=0$ is used for supplying the machine during these simulations as it was for the experimental tests (as presented in the Fig. 4). The obtained results for each amplitude of magnetization currents are presented in the Table II. A flowchart summarizing the steps of the model proposed for validating the experimental tests is presented in the Fig. 8.

For verifying by simulation, the hypothesis of a sinusoidal back-EMF measured in the VFMM during the experimental tests, the recoil lines presented in the Table II are used for characterizing the rotor. The flux linkage per phase (λ_s , in Wb) can be calculated in no-load condition according to the mechanical position of the rotor (θ , in radians). Then, using the Faraday's Law, the back-EMF at $\omega=45krpm$, same regime of the experimental tests, can be calculated by

$$E = -\frac{d\lambda}{dt} = -\frac{d\lambda}{d\theta} \frac{d\theta}{dt} = -\frac{d\lambda}{d\theta} \omega \quad (5)$$

Considering the recoil line obtained for $I_{mag}=800A$ ($B_r=0.147T$, $H_c=-8.0kA/m$ and $\mu_r=14.65$), it is obtained a peak flux linkage of $\lambda_s=57.97\mu Wb$ and a back-EMF of amplitude

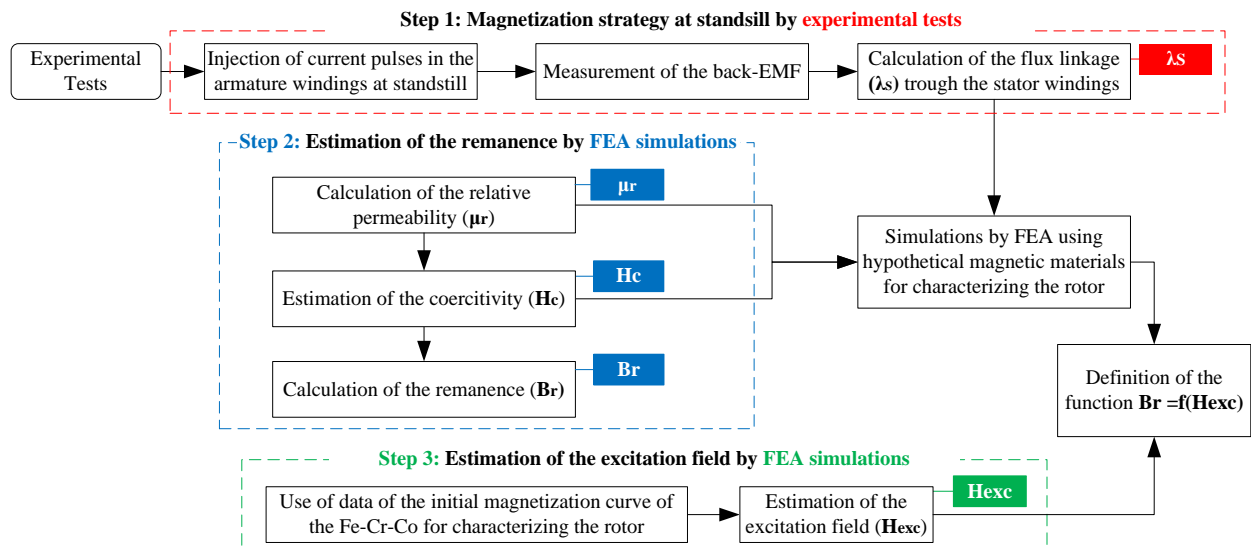


Fig. 8. Overview of the methodology proposed for validating the working point placement of the Fe-Cr-Co

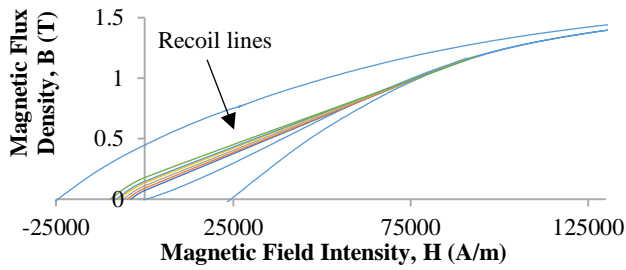


Fig. 10. Hysteresis loops obtained by simulations from experimental results using the methodology proposed for the Fe-Cr-Co inserted in the VFMM

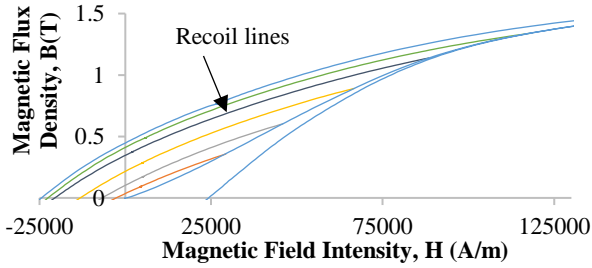


Fig. 11. Hysteresis loops obtained by experimental tests using the HysteresisGraph for a sample of Fe-Cr-Co magnet

$E_{pp}=929.8\text{mV}$, as shown in the Fig.9. This last result represents an error of 2.7% when compared to the one obtained by the experimental tests, as presented in the Fig.6. Therefore, the back-EMF can be considered sinusoidal.

E. Evaluation of the results obtained from methodology proposed

In the Fig. 10, the recoil lines obtained by simulations from the experimental results using the methodology presented in the Fig.8 are exhibited. For studying the intrinsic magnetic behavior of the magnet recoil lines, a sample of Fe-Cr-Co is characterized by a HysteresisGraph. Fig. 11 shows the achieved results. From these, it can be observed that the minor loops present a parallel behavior to the major demagnetization curve in the second quadrant, as expected. Also, it is noticed that different coercivities characterize each recoil line. This characteristic represents the main difference to the magnetic behavior observed when the Al-Ni-Co magnets are used.

Even if the shape of the recoil lines exhibited in both Fig. 10 and Fig. 11 are similar, the ones estimated by using the methodology proposed have a higher relative permeability

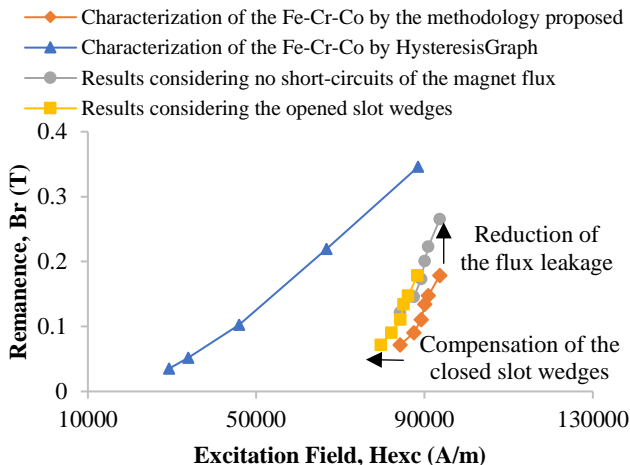


Fig. 12. Remanence in terms the excitation field in the Fe-Cr-Co magnet ($B_r=f(H_{exc})$)

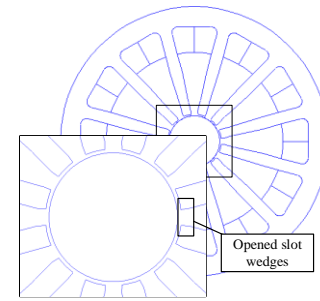


Fig. 13. Machine geometry considering opened slot wedges

(higher slope). Consequently, from a same level of excitation field achieved in the initial magnetization curve of both mentioned B-H-loops, lower remanences are seen for the recoil lines in the Fig. 10. This difference between the results presented in the Fig. 10 and Fig. 11 can be more clearly observed by means of the curves of $B_r=f(H_{exc})$ presented in the Fig. 12.

Investigations revealed that three major factors justify the differences observed in the Fig.12. First, as previously discussed, a HysteresisGraph is a closed and ideal magnetic circuit of measurement, designed to measure the intrinsic magnetic properties of a magnet without interfere in the results obtained (without flux leakage). Therefore, it provides a path of low reluctance that forces all the flux lines crossing the equipment during the experimental tests to pass through the magnet. For the VFMM presented in the Fig.1 however, simulations results show that the closed slot wedges in the stator, when no saturated, are an alternative path for the flux lines during the initial magnetization process. When the stator ampere-turns are sufficient for saturating these regions, the major part of the flux lines pass through the rotor, ensuring the magnetization of the Fe-Cr-Co. Therefore, the closed wedges deviate a part of the magnetic flux lines, which leads to a requirement of higher ampere-turns for magnetizing the rotor. In this regard, for being crossed by a same flux, the magnet inserted in the HysteresisGraph require less ampere-turns, as it was observed in the Fig.12. For better understanding this behavior, the excitation of the VFMM studied in this paper is compared to the one of a similar geometry, in which the slot wedges are opened, as shown in the Fig.13. For this new geometry, the remaining design characteristics are preserved, and the magnetic behavior is closer to the one exhibited by the HysteresisGraph. Simulations demonstrate that for achieving a same magnet flux density, lower ampere-turns (in this case, lower I_{mag}) are required for the machine designed by opened slot wedges. These results can be analyzed in the Table III support the behavior observed in the Fig. 12.

TABLE III
STUDY OF THE EFFECTS OF THE CLOSED SLOT WEDGES IN THE STATOR GEOMETRY BY FEA SIMULATIONS

Magnet flux density B (T)	Magnetization currents amplitude (I_{mag}) [A_{pk}]	
	Closed slot wedges geometry	Opened slot wedges geometry
1.089	500	420
1.146	700	520
1.182	900	620

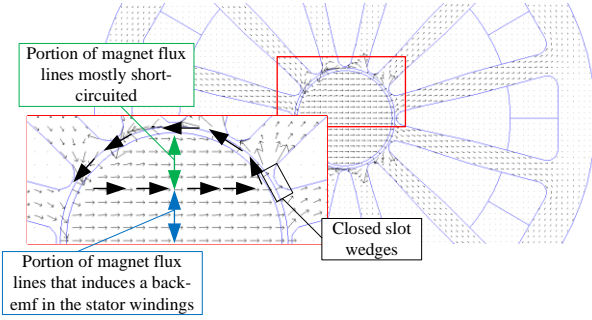


Fig. 14. Short-circuit of the magnet flux lines observed from simulations by the vector plot

From this analysis, compensating the effects of having a design composed of closed slot wedges, the obtained results are closer to the ones achieved by the HysteresisGraph, as shown in the Fig.12.

Until concerning the machine geometry, as previously mentioned, the stator was initially designed for a PMSM. The Nd-Fe-B magnet equipping this PMSM has a high level of remanence (of around 1.2T), which is sufficient to saturate the closed slot wedges present in the stator geometry when the machine at standstill (after magnetization). As previously discussed, when the closed slot wedges are saturated, all the magnet flux lines will cross the stator teeth. Rotating the machine at no load ($I_{\text{mag}}=0\text{A}$), this flux will induce a back-EMF in the armature windings, which are going to be measured during the experimental tests. Nevertheless, for the VFMM, because of the low remanence of the Fe-Cr-Co magnet used, fixed at 0.45T for the major hysteresis loop and even lower values for the recoil lines presented in the Table II, these regions are not saturated.

Thus, part of the magnet flux is short-circuited by the path provided by the slot wedges, which reduces the portion of magnet that contributes to the generation of back-EMF. The Fig. 14 presents this effect in the VFMM which rotor is characterized using the recoil line obtained when the machine is magnetized by $I_{\text{mag}}=900\text{A}$ (presented in the Table II). Analysis demonstrate that the leakages represents almost 40% of the total magnet flux. Applying the methodology proposed for a condition which the magnet flux is totally used in the stator windings for the back-EMF generation, the results presented in the Fig.12 can be obtained. It is concluded that considering null the flux leakage through the wedges approximates the obtained results to the reference ones, achieved using the HysteresisGraph.

The second difference between the results obtained from the HysteresisGraph and the methodology proposed is that the magnetic circuit composing the measuring equipment cannot be saturated, only the magnet sample. For the VFMM, however, these effects of saturation can be present in the stator teeth and yoke, according to the amplitude of currents injected in the armature windings. As these mentioned currents are high for initially magnetizing the rotor, the ampere-turns necessary for achieving the expected level of magnet flux density are considerably higher that should be without the stator saturation.

Finally, as already mentioned, the HysteresisGraph is a closed magnetic circuit of measurement. Because of this characteristic, an external excitation field applied for characterizing the magnet inserted in this equipment is equal to the internal field of the magnet (H_m , in A/m), as all the flux lines

that cross the steel core also pass through the magnet. This, however, is not the case for the VFMM studied in this paper. For a magnet inserted in this machine, due to the flux leakage that makes the system closer to an open circuit, an effect of self-demagnetization field (H_d , in A/m) is induced [15][17]. This last mentioned presents of opposite direction to the magnetization M , being approximately calculated by [15]-[18]:

$$H_d = -N_d M \quad (5)$$

where N_d is the demagnetizing factor, calculated according to the magnet shape. Studies as [17] and [18] are focused on the calculation of the demagnetizing factor for different sample shapes. Reference [19] discusses the importance of the shape of Al-Ni-Co magnets in their magnetization. According to the authors, differently than what is observed for some hard magnets as the Sm-Co, soft magnets as the Al-Ni-Co have shape-dependent retention of magnetization due the self-demagnetization field effect. For this reason, these soft magnets are commonly manufactured as short bars or squat horseshoes. For the VFMM studied in this paper, the stator geometry, designed with closed slot wedges, and the characteristics of saturation of the steel on it, impacts the flux leakage. Therefore, it contributes to making the system closer to an open circuit of measurement, as discussed previously and possibly increase the effects of self-demagnetization present in the magnet. This might explain the last differences between the experimental and the HysteresisGraph results. As analyzed in [20] for hard magnets, due to the contributions of a demagnetizing field, the slope of hysteresis curves obtained by an open magnetic circuit is different to the one obtained by a closed magnetic circuit as the HysteresisGraph. Nevertheless, it is the mathematical development for calculating the demagnetizing factor is not the focus of this paper.

III. CONCLUSION

The variation of the magnetization achieved by supplying a Fe-Cr-Co-based VFMM by d-axis current pulses at standstill is explored in this paper. The Fe-Cr-Co magnet equipping this machine is a low coercive force magnet with no well-defined knee in the second quadrant of the hysteresis curve. As consequence, the methodology commonly used in the literature for defining the behavior of the recoil lines in similar magnets as the Al-Ni-Co ones cannot be directly used. For this reason, a new methodology is proposed in this paper. The hypothesis of parallelism between both major and minor hysteresis loops is used for defining the behavior of the recoil lines of the Fe-Cr-Co magnet. By comparing the obtained results with the ones achieved using a HysteresisGraph, it is observed that the recoil lines obtained by these both characterization methods present a similar shape. Nevertheless, some differences between them should be discussed. First, analysis demonstrated that a higher excitation field is measured in the magnet inserted in the considered machine, because of the closed slot wedges of its stator should be saturated before the flux lines excitate the magnet. Also because of the stator geometry, a magnet leakage flux is present during the measurement of the back-EMF at standstill, which reduces the flux linkage through the stator

windings. The stator saturation is also a important point for justifying the differences observed between the results obtained by the methodology proposed and the ones achieved using the HysteresisGraph. The yoke and stator teeth saturate during the initial magnetization of the magnet. Because of this effect, that is present in the VFMM, but not in the measuring equipment, higher levels of ampere-turns are required for magnetizing the magnet. Additionally, the reduction of the excitation field estimated by the methodology discussed can be justified by the magnet shape effects which induces a self-demagnetization of the magnet equipping the considered machine.

REFERENCES

- [1] V. Ostovic, "Memory motors," in *IEEE Industry Applications Magazine*, vol. 9, no. 1, pp. 52-61, Jan.-Feb. 2003.
- [2] R. Jayarajan, N. Fernando and I. U. Nutkani, "A Review on Variable Flux Machine Technology: Topologies, Control Strategies and Magnetic Materials," in *IEEE Access*, vol. 7, pp. 70141-70156, 2019.
- [3] A. M. Aljehaimi and P. Pillay, "Operating envelopes of the variable-flux machine with positive reluctance torque," in *IEEE Transactions on Transportation Electrification*, vol. 4, no. 3, pp. 707-719, Sept. 2018.
- [4] H. Hua, Z. Q. Zhu, A. Pride, R. Deodhar and T. Sasaki, "Comparative study on variable flux memory machines with parallel or series hybrid magnets," in *IEEE Transactions on Industry Applications*, vol. 55, no. 2, pp. 1408-1419, March-April 2019.
- [5] H. Tahanian, M. Aliahmadi and J. Faiz, "Ferrite Permanent Magnets in Electrical Machines: Opportunities and Challenges of a Non-Rare-Earth Alternative," in *IEEE Transactions on Magnetics*, vol. 56, no. 3, pp. 1-20, March 2020.
- [6] J. Widmer, R. Martin, M. Kimiabeigi, "Electric vehicle traction motors without rare earth magnets," in *Sustainable Materials and Technologies*, vol.3, pp 7-13, 2015.
- [7] Z. Li, A. Kedous-Lebouc, J.-. Dubus, L. Garbuio, S. Personnaz, "Direct reuse strategies of rare earth permanent magnets for PM electrical machines – an overview study," in *European Physical Journal: Applied Physics*, EDP Sciences, vol. 86 no.2, pp.20901, 2019.
- [8] C. Yu, S. Niu, S. L. Ho, W. Fu and L. Li, "Hysteresis modeling in transient analysis of electric motors with AlNiCo magnets," in *IEEE Transactions on Magnetics*, vol. 51, no. 3, pp. 1-4, March 2015.
- [9] S. Jin, "Deformation-induced anisotropic Cr-Co-Fe permanent magnet alloys," in *IEEE Transactions on Magnetics*, vol. 15, no. 6, pp. 1748-1750, November 1979.
- [10] R. Owen, Z. Q. Zhu, J. B. Wang, D. A. Stone and I. Urquhart, "Review of variable-flux permanent magnet machines," in *2011 International Conference on Electrical Machines and Systems*, pp. 1-6, 2011.
- [11] B. Basnet, A. M. Aljehaimi and P. Pillay, "Back-EMF Analysis of a Variable Flux Machine for Different Magnetization States," in *IEEE Transactions on Industrial Electronics*, vol. 68, no. 10, pp. 9125-9135, Oct. 2021.
- [12] H. Yang, H. Lin and Z. Q. Zhu, "Recent advances in variable flux memory machines for traction applications: A review," in *CES Transactions on Electrical Machines and Systems*, vol. 2, no. 1, pp. 34-50, March 2018.
- [13] C. Yu and K. T. Chau, "Design, Analysis, and Control of DC-Excited Memory Motors," in *IEEE Transactions on Energy Conversion*, vol. 26, no. 2, pp. 479-489, June 2011.
- [14] F. Fiorillo, "Measurements of Magnetic Materials," in *Metrologia*, vol. 47, no. 2, S114, 2010.
- [15] R. Groessinger, "Characterisation of hard magnetic materials," in *Journal of ELECTRICAL ENGINEERING*, vol. 59, no.7/s pp.15-20, 2008.
- [16] F. D. de Sousa, A. Battiston, S. Pierfederici and F. Meibody-Tabar, "Validation of the standstill magnetization strategy of a FeCrCo-based Variable Flux Memory Machine," *2021 23rd International Conference on Electrical Machines and Systems (ICEMS)*, submitted for publication.
- [17] R. Prozorov and V. Kogan, "Effective Demagnetization Factors of Diamagnetic Samples of Various Shapes," in *Physical Review Applied*, vol.10, no. 1, July 2018.
- [18] B. K. Pugh, D. P. Kramer and C. H. Chen, "Demagnetizing Factors for Various Geometries Precisely Determined Using 3-D Electromagnetic Field Simulation," in *IEEE Transactions on Magnetics*, vol. 47, no. 10, pp. 4100-4103, October 2011.
- [19] R. Skomski, J.M.D. Coey, "Magnetic anisotropy — How much is enough for a permanent magnet?," in *Scripta Materialia*, vol. 112, pp 3-8, February 2016
- [20] J. Fliegans, G. Delette, A. N. Dobrynin, N. M. Dempsey and D. Givord, "Closed-Circuit Versus Open-Circuit Characterization of Hard Magnets," in *IEEE Transactions on Magnetics*, vol. 55, no. 2, pp. 1-5, Feb. 2019, Art no. 2101105.

Flavia Domingues de Sousa received the M.Sc. degrees in electrical engineering and power electronics from the Federal University of Minas Gerais (UFMG), Minas Gerais, Brazil, in 2019. She is currently a Ph.D. student with the Laboratory LEMTA of the University of Lorraine and the IFP Energies Nouvelles. Her research interests include variable flux memory machines, power electronics and control.

Alexandre Battiston received the Ph.D. degree in electrical engineering from the university of Lorraine, Nancy, France in 2014. He joined the IFP Energies Nouvelles, Rueil-Malmaison, France, in October 2014, where he is currently a research engineer in power electronics at the mechatronic and numeric department. His research interests include power electronics architectures & controls and their applications.

Farid Meibody-Tabar received the Engineer degree from the Ecole Nationale d'Electricite et de Mecanique de Nancy, Nancy, France, in 1982, and the Ph.D. and Habilitation a diriger des recherches degrees from the Institut National Polytechnique de Lorraine (INPL), Nancy, France, in 1986 and 2000, respectively. Since 2000, he has been a Professor at INPL. His research activities in the Groupe de Recherche en Electronique et en Electrotechnique de Nancy (GREEN), Institut National Polytechnique de Lorraine, Vandoeuvre-Les-Nancy, France, deal with electric machines, their supply, and their control.

Serge Pierfederici received the Dipl.-Ing from the Ecole Nationale Supérieure d'Electricité et Mécanique, Nancy, France, in 1994, and the Ph.D. degree in electrical engineering from the Institut National Polytechnique de Lorraine, Nancy, France, in 1998. Since 2009, he has been a Full Professor with the University of Lorraine, Nancy, France. He is the main author and also the co-author of more than 200 papers that were published in the international peer-reviewed journals. His research interests include the stability study of distributed power systems and modeling and control of power electronic systems. His current research interests include the distributed control of multisources and multicarrier microgrids. Dr. Pierfederici is currently on the editorial boards of the international peerreviewed journals. He was the recipient of several IEEE awards.